



Journal Name

ARTICLE

Low-surface-area nitrogen doped carbon nanomaterial for advanced sodium ion batteries

Chaokun Liu, Jiangtao Hu, Luyi Yang, Wenguang Zhao, Hejie Li and Feng Pan*

Received 00th January 20xx,
Accepted 00th January 20xx

DOI: 10.1039/x0xx00000x

www.rsc.org/

Low-surface-area nitrogen-doped carbon nanomaterial was prepared via a facile annealing method, which shows good Na-ion storage ability (334 mA g⁻¹) and coulombic efficiency due to its mixed charge-discharge mechanism and unique structural features.

Among various energy storage devices, rechargeable lithium-ion batteries (LIBs) are intensively studied as power sources for consumer portable electronic devices, owing to their high specific capacity, rate capacity and cycling stability.^{1,2} However, the high cost and limited terrestrial reserves of lithium may restrict LIBs' applications for large-scale energy storage.^{3,4} Therefore, attention is starting to shift to exploring alternative energy storage technologies. Na-ion batteries (SIBs), which have already become one of the most attractive low-cost alternative to LIBs due to the abundant supply and wide distribution of sodium resources.⁵ In recent years, significant progress has been made in the field of cathode materials for SIBs.^{6,7} Correspondingly, there are also several anode materials, such as metal oxides,^{8,9} alloys,¹⁰ and carbonaceous materials,¹¹ have been investigated for SIBs. Since transition metal oxide spinel NiCo₂O₄ was first reported as an anode for SIBs in 2002,⁸ many metal oxide such as Fe₂O₃¹², SnO₂¹³, CO₂O₃¹⁴ and CuO¹⁵ have been investigated as anodes for SIBs. However, the relatively low initial coulombic efficiency, poor electronic conductivity, large hysteresis and enormous volume expansion have limited the application of metal oxide though they exhibit high capacity and energy densities.^{16,17} Therefore, carbonaceous materials are regarded as the most promising candidate for SIBs due to their abundance, thermal stability and low price similar to anode materials for LIBs. However, graphite, which is used as the commercial LIB anode, exhibits extremely low capacity of 31 mAh g⁻¹ for Na-ion storage.¹⁸ This is due to that in LIBs, the formation of a series of binary graphite intercalation compounds (b-GIC) allows the reversible intercalation of Li-ions¹⁹ while this mechanism cannot be applied to SIBs due to the

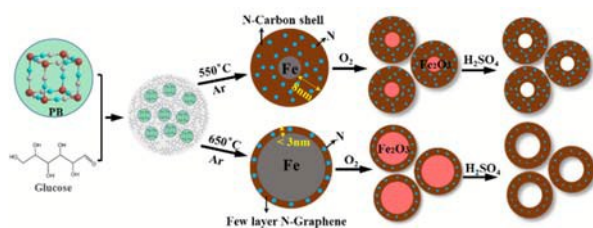
lack of suitable binary intercalation compounds.¹⁸ The mismatch between the Na ion and graphite structure leads to no existence of b-GICs under moderate conditions.^{20,21} To overcome these issues, many other carbonaceous materials have been proposed, including hollow carbon nanowires/nanospheres,²² carbon nanotubes (CNTs),²³ and porous carbon fibers, possessing a larger interlayer spacing with various morphologies and structures to obtain a higher capacity in Na-ion storage.²⁴ Introduction of nitrogen atoms is considered as an effective way to improve the electrochemical performance for Na-ion batteries, which can both enhance the electric conductivity and capacity.^{25,26} It is also reported that nitrogen doping can generate a pseudo-capacitance due to the interaction between the electrolyte and N species on the surface.²⁷ For example, Cao *et al.* investigated hollow carbon nanowires derived from polyaniline,²² which can deliver a reversible capacity of 251 mA h g⁻¹ with a 50.5% initial coulombic efficiency. Wang *et al.* synthesized porous N-doped nanosheets from graphene oxide (GO), showing a reversible capacity of 200 mA h g⁻¹ after 250 cycles at a current density of 50 mA g⁻¹.²⁸ The studies described above have showed that N-doped porous carbon materials generally exhibit good rate and cycling capability, but the initial coulombic efficiency is typically very low due to the more prominent formation of solid electrolyte interphase (SEI) layer on the large surface.²⁹ Therefore, a facile method to synthesis N-doped carbon with high capacity and low surface area is desired. Herein, we report a low-surface-area carbonaceous derivative from Prussian Blue (PB) with rich nitrogen doping, which can exhibit high reversible capacity (334 mA h g⁻¹ at 0.05 A g⁻¹), excellent cycling performance (212 mA h g⁻¹ after 200 cycles at the current density of 0.01 A g⁻¹) and high initial coulombic efficiency of 64.9%. In addition, the different Na-ion storage mechanisms of the samples annealed at different temperatures have been discussed.

As demonstrated in **Scheme 1**, nitrogen doped carbon nanomaterials were synthesized via a facile annealing method using PB as precursor (experimental details can be found in supplementary information). By applying different annealing temperatures (550 °C and 650 °C) under argon atmosphere, two types of nitrogen doped carbon (NC) can be resulted (NC-550 and NC-650).

School of Advanced Materials, Peking University Shenzhen Graduate School, Shenzhen 518055, China.

Email: panfeng@pkusz.edu.cn

Electronic Supplementary Information (ESI) available: [Experimental details; XPS data; kinetic analysis of CV]. See DOI: 10.1039/x0xx00000x



Scheme 1 Formation process of different nitrogen-doped hollow carbon shells (NC-550 and NC-650).

Morphology and structure characteristics of NC-550 and NC-650 are investigated by the scanning electron microscopy (SEM) and the transmission electron microscopy (TEM). In the SEM image of NC-550 (Fig. 1a), it can be observed that NC-550 consists of blocky-shaped particles with diameters around 10~30 μm , which shows smooth surfaces with few honeycomb-like structures exposed to the surface. While as shown in Fig. 1d, NC-650 exhibits a much rougher surface indicating a porous structure. Images under higher magnification were taken to further investigate the crystalline structure of the samples. From the TEM images, NC-550 (Fig. 1b and 1c) clearly demonstrate that it has a relatively ordered macroporous feature with arranged thick graphene layers, which not only allows electrolyte permeation and but also enhances sodium ion transfer rate between the electrode and electrolyte.²⁹

X-ray diffraction (XRD) patterns are collected to study the crystallinity information of the final two samples (Fig. 2a). Both NC-550 and NC-650 exhibit two broad peaks at around 25.8° and 43.0° on XRD spectrum, which can be indexed to (002) and (101) planes respectively. Notably, N-550 shows a weak peak at 26.5°, indicating the presence of crystalline carbon or graphite-like structure and a small d_{002} spacing of 0.34 nm. Compared to NC-650, NC-550 contains more graphite-like domain which is transformed from graphene layers.²³ N_2 adsorption-desorption isotherms of NC-550 and NC-650 (Fig. 2b) both show typical type IV shape with H_3 hysteresis, indicating the presence of mesopores.²⁵ NC-650 shows a high Brunauer-Emmett-Teller (BET) surface area of 553.2 $\text{m}^2 \text{g}^{-1}$ while the NC-550 only shows a much lower specific surface area of 12.1 $\text{m}^2 \text{g}^{-1}$.

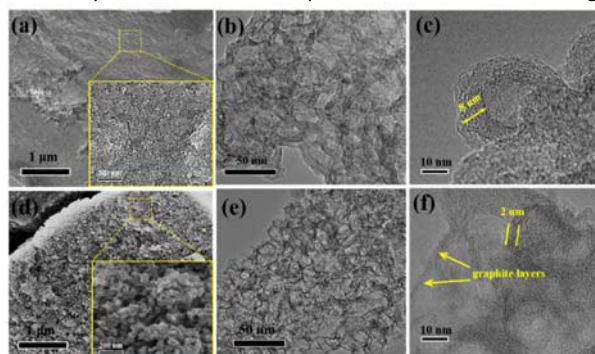


Fig. 1 SEM and images of NC-550 (a) and NC-650 (d); TEM images of NC-550 (b, c) and NC-650 (e, f).

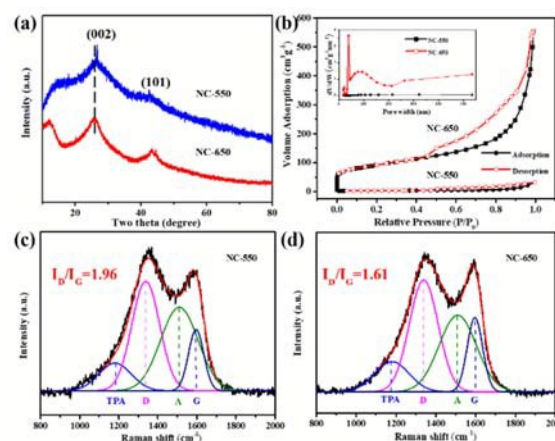


Fig. 2 (a) XRD data of NC-550 and NC-650; (b) N_2 adsorption/desorption isotherms of NC-550 and NC-650; Raman spectra of NC-550 (c) and NC-650 (d), which are fitted into four Lorentzian peaks.

According to the pore size distribution curves (Fig. 2b, inset), NC-550 mainly consists of macropore and few mesopores and NC-650 shows a high content of mesopores, implying the Fe^{3+} in PB has different catalytic effects on the formation of graphene layers at different temperature. Furthermore, Raman spectra of NC-550 and NC-650 between 800 and 2000 cm^{-1} are measured to calculate the coherence lengths of graphenic domains (L_a) according to the following equation:

$$L_a \text{ (nm)} = (2.4 \times 10^{-10}) \lambda_{nm}^4 \left(\frac{I_G}{I_D}\right) \quad (1)$$

where λ_{nm} is 514 nm, and I_G and I_D are intensity of the G band and D band, where the D band at $\approx 1350 \text{ cm}^{-1}$ can be attributed to the A1g vibration of finite-sized graphitic domains and the G-band at $\approx 1600 \text{ cm}^{-1}$ is resulted from the Eg2 vibration of sp^2 carbon.²⁶ Two broad peaks in Raman spectra of NC-550 and NC-650 can be fitted into four Lorentzian peaks to identify D and G bands accurately as shown in Fig. 2c and Fig. 2d. According to Equation (1), L_a values of NC-550 and NC-650 are calculated to be 8.48 nm and 10.81 nm, respectively. The shorter coherence length of graphenic domains for NC-550 suggests that graphenic layers in NC-550 may be shorter or more curved. Moreover, the ratio of I_D to I_G can also be considered as an indication of defect concentration.³⁰ Therefore, it can be deduced that NC-550 contains higher concentration of defects due to a higher ratio (1.96) than that of NC-650 (1.61). It can be concluded that NC-550 has a lower degree of graphitization, which is reported to be advantageous in Na^+ storage.^{31,32}

Recent studies have shown that the nitrogen doping in carbon-based anodes plays an important role in the electrochemical performance of SIBs. Nitrogen dopants not only improve the electrical conductivity of carbon, but also generate extrinsic defects to support active Na storage sites.^{25,26} X-ray photoelectron spectroscopy (XPS) measurements also were carried out to analyse the different functional groups in NC-650 and NC-550 (shown in Fig.

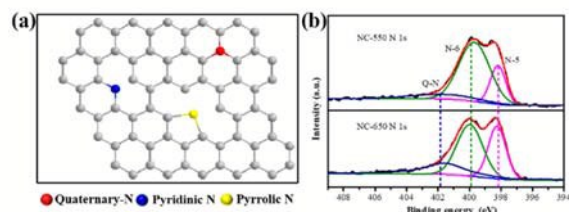


Fig. 3 (a) N 1s XPS survey spectra of NC-550 and NC-650 with fittings; (b) schematic figure of different types of N in carbon.

S1). From **Table S1** it can be seen that the atomic contents of nitrogen for NC-650 and NC-550 are 12.8% and 15.9%, respectively. XPS data have been further analyzed, XPS fitting was carried out for N 1s spectra. **Fig. 3a** shows three types of N atoms: pyridinic N (N-6), pyrrolic N (N-5) and quaternary N (N-Q). N-5 and N-6 are defective sites and usually considered as electro-active for Na storage.³³ From **Fig. 3b**, it can be seen that pyridinic N (N-6, 398.4 ± 0.2 eV) and pyrrolic N (N-5, 399.8 ± 0.2 eV) are dominant components in both samples. The total atomic content of pyridinic and pyrrolic N in the NC-550 and NC-650 are 90.5% and 77%, respectively. The higher content for defective N sites in NC-550 could be beneficial for its electrochemical performance.

To examine their electrochemical properties, NC-550 and NC-650 have also been fabricated into electrodes for Na-ion half-cells. **Fig. 4a** shows the first-cycle voltage profiles of NC-550 and NC-650 electrodes at the current density of 50 mA g^{-1} . The electrode of NC-550 and NC-650 delivers reversible specific capacities of 373 and 292 mA h g^{-1} with initial coulombic efficiency of 64.9% and 24.3%, respectively. The large irreversible capacity loss for NC-650 results from the large degree of electrolyte decomposition and SEI layer formation on its large surface, while NC-550 exhibits a higher initial coulombic efficiency and reversible capacity of due to its unique structure with low surface, more active sites and higher disorder degree for sodium storage. Fig. 4b displays the rate performances of the NC-550 and NC-650 electrodes. The NC-650 exhibits a poor rate performance with a capacity of merely 110 mA h g^{-1} at a current density of 0.5 A g^{-1} , while the NC-550 delivered reversible capacities of 334, 317, 295, 276, 247 and 212 mA h g^{-1} at a current density of 50, 80, 100, 150, 250, 500 mA g^{-1} , respectively. And a reversible capacity of 315 mA h g^{-1} can be recovered as the current density reversed to 50 mA g^{-1} . In addition, as illustrated in **Fig. 4c**, a reversible capacity of 212 mA h g^{-1} (76.1% retention) was retained for the NC-550 electrode after 200 cycles at the density of 100 mA g^{-1} , which is twice of NC-650 (102 mA h g^{-1} , 55.7% retention), so NC-550 exhibits a better capacity retention ratio with a slightly capacity fading process compared with NC-650. After 200 cycles, a smaller charge-transfer impedance (R_{ct}) for NC-550 is demonstrated compared with NC-650 in the electrochemical impedance spectra (**Fig. 4d**), which is another evidence for less SEI formation on the NC-550 electrode. **Fig. 4a-4d** have showed that NC-550 possesses superior electrochemical properties compared to NC-650, which can be attributed to its unique structures demonstrated above including lower specific surface area, lower degree of graphitization and more active N-doping sites. Since NC-550 and NC-650 exhibit varied voltage profiles

(**Fig. S2**), it is of great importance to study their charge-discharge mechanisms.

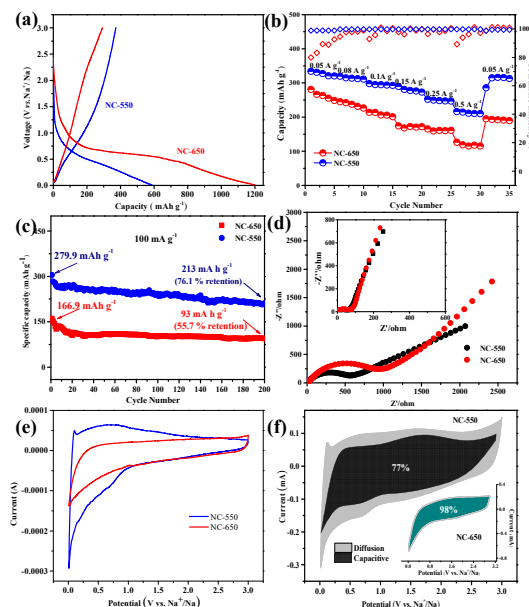


Fig. 4 (a) First-cycle voltage profiles of two samples at a current rate of 50 mA g^{-1} ; (b) Cycling performance of NC-550 and NC-650 at different densities; (c) long term cycling performance of NC-550 and NC-650; (d) Nyquist plots of half cells with NC-550 and NC-650 before (inset) and after 200 cycles; (e) 2nd cyclic voltammograms of half cells at the scanning rate of 0.1 mV s^{-1} ; (f) capacitive charge storage contributions of NC-550 and NC-650 at a scan rate of 1 mV s^{-1} .

The cyclic voltammetry (CV) results of NC-550 and NC-650 are shown in **Fig. 4e**. It can be seen that during the anodic scan, NC-550 shows a sharp desodiation peak, which cannot be observed for NC-650, suggesting that the charge-discharge mechanisms for NC-550 and NC-650 might be different. Generally, the current collected from carbon-based anodes includes redox pseudo capacitive process generated at the surface of active materials and the diffusion-controlled process in the bulk of materials.³⁴ To further study the pseudo capacitance's contribution to the total Na-ion storage, CV curves at different current densities were applied. The contribution from capacitive effects and diffusion-controlled process can be represented as:

$$i(V) = k_1 v + k_2 v^{1/2} \quad (2)$$

where $i(V)$ represents the total current response at a given potential V , v is the scan rate, k_1 and k_2 are constants. Here, $k_1 v$ and $k_2 v^{1/2}$ correspond to the surface capacitive behaviour and the diffusion-controlled process, respectively. After interpreting the results from CV curves at different scan rates (details shown in **Fig. S3** and **S4**), the values of k_1 and k_2 can be determined in order to calculate the pseudo capacitive current contribution at a given potential. As shown in **Fig. 4f**, at the scan rate of 1 mV s^{-1} , the potential profiles for the current responses of capacitive effects are presented to compare with the total measured current area. A dominating capacitive contribution is 98% NC-650 electrode, indicating that the Na-ion storage is significantly associated with surface reaction. However,

the NC-550 electrode delivers a smaller pseudo capacitance storage (77%), indicating that the Na-ion storage is only partly related with surface reaction. To understand the kinetic origin, the degree of capacitive effect can be qualitatively analysed corresponding to the relationship between measured current (i) and scan rate (v) from CV curves:

$$i = av^b \quad (3)$$

where a and b are both constants. The value of b , generally found between 0.5 (diffusion limited) and 1.0 (surface capacitance-dominated), is determined from the slope of the $\log(i)$ vs $\log(v)$ curve (details shown in Fig. S5). The b -values of NC-550 at different potentials are between 0.5 and 1, indicating a mixture of both lithium semi-infinite linear diffusion and surface reaction. In contrast, the b -values of NC-650 are approximately unit at all potentials, indicating that the surface reaction contributes to almost 100% capacity of NC-650 due to its large surface area. As a result, it is believed that this mixed Na^+ storage mechanism of NC-550, which originates from its unique structure, is the main reason for the improved electrochemical performances.

To conclude, carbon nanosheets with relatively low specific surface area (NC-550) and high specific surface area (NC-650) were prepared and tested as anode material for SIBs. NC-550 exhibits a high initial coulombic efficiency (64.9%), reversible capacity (334 mA h g^{-1} at 50 mA g^{-1}) and excellent cycling performance (212 mA h g^{-1} after 200 cycles at 100 mA g^{-1}). The superior electrochemical properties of NC-550 can be attributed to its mixed charge-discharge mechanism, which is determined its structural features including lower specific surface area, lower degree of graphitization and more active N-doping sites. This promising approach can be further explored to acquire low-cost materials for sodium ion batteries. This work was financially supported by the National Materials Genome Project (2016YFB0700600), National Science Foundation of China (51602009), Guangdong Innovation Team Project (2013N080).

Conflicts of interest

There are no conflicts to declare.

Notes and references

- B. Dunn, H. Kamath and J.-M. Tarascon, *Science* (80-), 2011, **334**, 928–935.
- B. Scrosati, J. Hassoun and Y.-K. Sun, *Energy Environ. Sci.*, 2011, **4**, 3287.
- S. W. Kim, D. H. Seo, X. Ma, G. Ceder and K. Kang, *Adv. Energy Mater.*, 2012, **2**, 710–721.
- M. D. Slater, D. Kim, E. Lee and C. S. Johnson, *Adv. Funct. Mater.*, 2013, **23**, 947–958.
- D. A. Stevens and J. R. Dahn, *J. Electrochem. Soc.*, 2001, **148**, A803–A811.
- M. H. Han, E. Gonzalo, G. Singh and T. Rojo, *Energy Environ. Sci.*, 2015, **8**, 81–102.
- M. S. Islam and C. A. J. Fisher, *Chem. Soc. Rev.*, 2014, **43**, 185–204.
- R. Alcántara, M. Jaraba, P. Lavela and J. L. Tirado, *Chem. Mater.*, 2002, **14**, 2847–2848.
- Y. Sun, L. Zhao, H. Pan, X. Lu, L. Gu, Y. S. Hu, H. Li, M. Armand, Y. Ikumura, L. Chen and X. Huang, *Nat. Commun.*, 2013, **4**, 1810–1870.
- S. J. R. Prabakar, Y. H. Hwang, E. G. Bae, S. Shim, D. Kim, M. S. Lah, K. S. Sohn and M. Pyo, *Adv. Mater.*, 2013, **25**, 3307–3312.
- C. Zhu, X. Mu, P. A. Vanaken, Y. Yu and J. Maier, *Angew. Chemie - Int. Ed.*, 2014, **53**, 2152–2156.
- S. Komaba, T. Mikumo, N. Yabuuchi, A. Ogata, H. Yoshida and Y. Yamada, *J. Electrochem. Soc.*, 2010, **157**, A60.
- D. Su, X. Xie and G. Wang, *Chem. - A Eur. J.*, 2014, **20**, 3192–3197.
- M. M. Rahman, A. M. Glushenkov, T. Ramireddy and Y. Chen, *Chem. Commun.*, 2014, **50**, 5057–5060.
- L. Wang, K. Zhang, Z. Hu, W. Duan, F. Cheng and J. Chen, *Nano Res.*, 2014, **7**, 199–208.
- Y. H. Chao, J. S. Wu, C. E. Wu, J. F. Jheng, C. L. Wang and C. S. Hsu, *Adv. Energy Mater.*, 2013, **3**, 1279–1285.
- Y. Zhu, X. Han, Y. Xu, Y. Liu, S. Zheng, K. Xu, L. Hu and C. Wang, *ACS Nano*, 2013, **7**, 6378–6386.
- B. Jache and P. Adelhelm, *Angew. Chemie - Int. Ed.*, 2014, **53**, 10169–10173.
- G. Schmuelling, T. Placke, R. Kloepsch, O. Fromm, H. W. Meyer, S. Passerini and M. Winter, *J. Power Sources*, 2013, **239**, 563–571.
- K. Nobuhara, H. Nakayama, M. Nose, S. Nakanishi and H. Iba, *J. Power Sources*, 2013, **243**, 585–587.
- J. Sangster, *J. Phase Equilibria Diffus.*, 2007, **28**, 571–579.
- Y. Cao, L. Xiao, M. L. Sushko, W. Wang, B. Schwenzer, J. Xiao, Z. Nie, L. V. Saraf, Z. Yang and J. Liu, *Nano Lett.*, 2012, **12**, 3783–3787.
- I. Elizabeth, R. B. Mathur, P. H. Maheshwari, B. P. Singh and S. Gopukumar, *Electrochim. Acta*, 2015, **176**, 735–742.
- W. Luo, Z. Jian, Z. Xing, W. Wang, C. Bommier, M. M. Lerner and X. Ji, *ACS Cent. Sci.*, 2015, **1**, 516–522.
- H. Wang, C. Zhang, Z. Liu, L. Wang, P. Han, H. Xu, K. Zhang, S. Dong, J. Yao and G. Cui, *J. Mater. Chem.*, 2011, **21**, 5430.
- W. H. Shin, H. M. Jeong, B. G. Kim, J. K. Kang and J. W. Choi, *Nano Lett.*, 2012, **12**, 2283–2288.
- Y. Wu, S. Fang and Y. Jiang, *J. Mater. Chem.*, 1998, **8**, 2223–2227.
- F. Su, C. K. Poh, J. S. Chen, G. Xu, D. Wang, Q. Li, J. Lin and X. W. Lou, *Energy Environ. Sci.*, 2011, **4**, 717–724.
- H. G. Wang, Z. Wu, F. L. Meng, D. L. Ma, X. L. Huang, L. M. Wang and X. B. Zhang, *ChemSusChem*, 2013, **6**, 56–60.
- C. Hu, S. Sedghi, A. Silvestre-Albero, G. G. Andersson, A. Sharma, P. Pendleton, F. Rodríguez-Reinoso, K. Kaneko and M. J. Biggs, *Carbon N. Y.*, 2015, **85**, 147–158.
- C. Bommier, T. W. Surta, M. Dolgos and X. Ji, *Nano Lett.*, 2015, **15**, 5888–5892.
- B. Cao, H. Liu, B. Xu, Y. Lei, X. Chen and H. Song, *J. Mater. Chem. A*, 2016, **4**, 6472–6478.
- H. Liu, M. Jia, B. Cao, R. Chen, X. Lv, R. Tang, F. Wu and B. Xu, *J. Power Sources*, 2016, **319**, 195–201.
- W. Ren, K. Wang, J. Yang, R. Tan, J. Hu, H. Guo, Y. Duan, J. Zheng, Y. Lin and F. Pan, *J. Power Sources*, 2016, **331**, 232–239.